

## 3D printing of multiple container models and their trajectory tests in calm water

Yi Li<sup>1</sup>, Hanqi Yu<sup>2</sup>, Damon Smith<sup>3</sup>, M.M. Khonsari<sup>4</sup>,  
Ryan Thiel<sup>1</sup>, George Morrissey<sup>1</sup> and Xiaochuan Yu<sup>\*1</sup>

<sup>1</sup>Boysie Bollinger School of Naval Architecture and Marine Engineering, University of New Orleans, USA

<sup>2</sup>Department of Mathematics, University of New Orleans, USA

<sup>3</sup>Department of Mechanical Engineering, University of New Orleans, USA

<sup>4</sup>Department of Mechanical & Industrial Engineering, Louisiana State University, USA

(Received January 12, 2021, Revised March 2, 2022, Accepted March 10, 2022)

**Abstract.** More and more shipping containers are falling into the sea due to bad weather. Containers lost at sea negatively affect the shipping line, the trader and the consumer, and the environment. The question of locating and recovering dropped containers is a challenging engineering problem. Model-testing of small-scaled container models is proposed as an efficient way to investigate their falling trajectories to salvage them. In this study, we first build a standard 20-ft container model in SOLIDWORKS. Then, a three-dimensional (3D) geometric model in the STL (Standard Tessellation Language) format is exported to a Stratasys F170 Fused Deposition Modeling (FDM) printer. In total, six models were made of acrylonitrile styrene acrylate (ASA) and printed for the purpose of testing. They represent three different loading conditions with different densities and center of gravity (COG). Two samples for each condition were tested. The physical models were dropped into the towing tank of University of New Orleans (UNO). From the experimental tests, it is found that the impact of the initial position after sinking can cause a certain initial rolling velocity, which may have a great impact on the lateral displacement, and subsequently affect the final landing position. This series of model tests not only provide experimental data for the study of the trajectory of box-shape objects but also provide a valuable reference for maritime salvage operations and for the pipeline layout design.

**Keywords:** 3D printing; container model; Fused Deposition Modeling (FDM); maritime industry; trajectory

### 1. Introduction

Over the past 30 years, containerization has dominated the main market environment where shipping and logistics are operating. It has substantially changed the organizational and institutional relationships of global freight transport. Bernhofen *et al.* (2015) were the first to propose an identification strategy for estimating the impact of the container revolution on global trade. However, the shipping industry is experiencing the biggest spike in lost containers. More than 3,000 boxes were dropped into the sea last year, and more than 1,000 have fallen overboard so far in 2021 (Koh 2021). There are a host of reasons for the sudden rise in accidents. While unpredictable weather is

---

\*Corresponding author, Associate Professor, E-mail: xyu5@uno.edu

the main reason, the situation is exacerbated by a surge in e-commerce after consumer demand exploded during the pandemic due to the urgency for shipping lines to deliver products as quickly as possible.

From the perspective of experimental tests in naval architecture and ocean engineering, carrying out container model tests can provide a reliable theoretical basis for studying the falling trajectory of the containers fallen overboard. However, working with conventional containers made of wood or those manufactured by metal mold is time-consuming, labor-intensive, and costly. Toward this need, additive manufacturing (AM) (also called “3D printing”) provides a fast, efficient, and more economical way to make small-scale models for various maritime structures (ABS 2017, Milewski 2017). This technology has applications in jewelry, industrial design, architecture, aerospace, dental and medical industries, education, civil engineering, and many other fields (Baumers *et al.*, 2016). It has the advantage of design freedom, mass customization, waste minimization and the ability to manufacture complicated structures, as well as rapid prototyping.

AM started to challenge the traditional method of modeling plastic materials since it is more economically achievable and environmentally friendly than injection molding and other traditional methods (Baumers *et al.* 2016, Ford and Despeisse 2016, Franchetti and Kress 2016). Ngo *et al.* (2018) outlined 3D printing, including a survey of its advantages and disadvantages, as a benchmark for future research and development. Arnold *et al.* (2021) used shrimp shell waste obtained from Louisiana Gulf shrimp as raw material to make the composite filaments and assess its use as a manufacturing material. Arnold *et al.* (2020) found that the composite filament of polylactic acid and fused filament fabrication can be directly used to make phantoms for education and preoperative planning.

As for the offshore industry, dropped objects may cause damage to subsea pipelines, thus affecting hydrocarbons transportation in offshore oil and gas development. Learning the trajectory of dropped containers will help determine their landing locations, as well as prevent the occurrence of hazards to submarine pipelines (DNV 2010). There are some experimental and numerical studies about the falling pattern of cylindrical objects, such as Aanesland (1987), Xiang *et al.* (2016), Xiang and Xiang (2021), Yu *et al.* (2019, 2020a, b), etc. However, there are very few studies about the dropped containers. In the maritime industry, the actual number of lost containers is difficult to determine and estimates of the scope of the incident are wide-ranging (Frey and DeVogelaere 2014). The experimental results in this paper can help to narrow the scope of salvage quickly, which can potentially save search time and thus reduce the overall salvage cost will help identify the loss caused by accidents, determine whether it is necessary to salvage the containers, and estimate the cost of manpower and material resources required.

The first objective is to apply the 3D printing technology to fabricate several small-scale container models; the second objective is to experimentally study the trajectories and landing locations of dropped container models in calm water. In addition, it should be addressed that the water-entry itself is not the focus of this paper, including the velocity and pressure distribution, etc. In fact, usually when one container drops, it will be flooded with water very quickly, and such process can change the submerged weight. The container may even collapse due to overpressure. There are so many factors to be considered when preparing these experimental tests. To simply our problem, we consider the dropped container model being fully flooded in the water with submerged weight and ignore the possibility of damage. We will focus on the trajectories of dropped container models after sinking.

Fig. 1 shows a flowchart about the major five steps to be implemented in this study. First, we use commercial software, SolidWorks, to construct 3D geometrical models. In this design stage, we

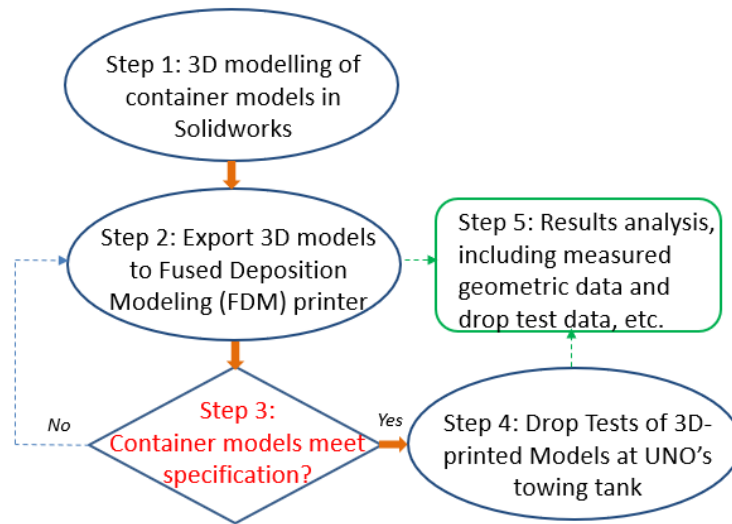


Fig. 1 Flowchart for major steps

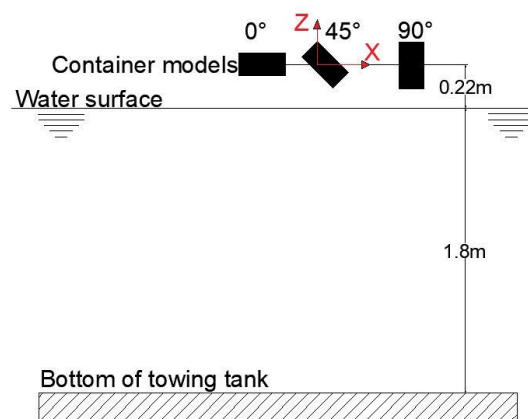


Fig. 2 A schematic view of drop test plan

insert a hole in different positions to adjust the average density and center of gravity (COG) by filling different high-density heavy metals to represent different loading conditions of containers. Next, these geometric models are then exported to a Stratasys F170 Fused Deposition Modeling (FDM) printer. In total, six models were made of acrylonitrile styrene acrylate (ASA) and printed for the purpose of testing. They represent three different loading conditions with different densities and COG, and there are two samples for each condition. The third step is to measure the geometric dimensions of the 3D-printed models and measure and estimate their COG to see if they meet our design requirements and other specifications, such as ABS (2018). This step is also important for 3D printing quality control.

After measuring and determining the basic parameters of these six models, we dropped four models with a density greater than water into UNO's towing tank and performed a series of drop tests to obtain data on the fall and the trajectory of these physical models after entering the water.

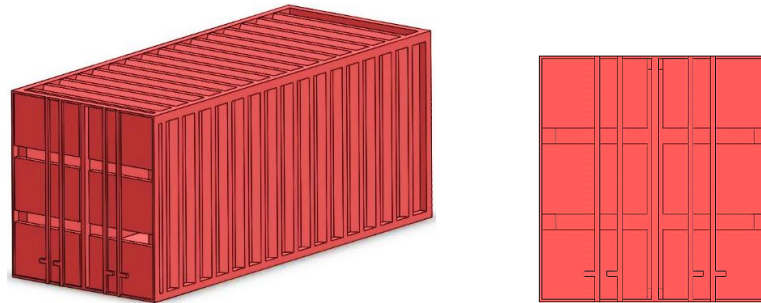


Fig. 3 The same front view for all the three types of container model- Model Type I, Model Type II and Model Type III

Fig. 2 shows a schematic view of the drop test plan. Finally, all the collected data, including the 3D printing data, the measurement data of 3D printed models, and the data from drop tests, will be finally analyzed.

It should be addressed in advance is that in the experimental tests, the time interval between each drop is long enough, so ideally the influence of water waves can be ignored.

## 2. Methods and procedures

### 2.1 3D Model in solidworks

Generally, there are 14 different most common types of containers, including dry containers, side open storage containers, half-height containers, drums, etc. (Chawa and Mukkamala 2018). In this paper, the standard 20 ft dry container is selected to be scaled with the ratio 35.69:1. The container wall thickness does not use this scale ratio, otherwise, the thickness obtained is too small to be achieved and does not meet the requirements of this experiment. In addition, the main purpose of this experiment is to determine the trajectory of the container model. Therefore, the destruction of the container model itself is not considered. Based on these assumptions, we use a solid model, which is slightly different from the actual container model. Considering that the 3D Printed model can quickly and accurately provide models with different centers of gravity and different densities, this is completely negligible.

This design was finalized after some consideration, including the maximum allowable dimensions of the FDM printer. As a result, the finalized size of the container model is  $169 \times 68 \times 72$  mm (Length  $\times$  Width  $\times$  Height). Table 1 gives the dimension of the original and the scaled container.

To construct the container models with different weights and centers of gravity, we design containers with a hole of 25 mm in diameter and 50 mm in depth placed in the middle and upper of models, respectively. To achieve this, we can fill the holes with different materials to change the weight and COG with centric hole (Fig. 4), type II - scaled model with eccentric hole (Fig. 5), and type III - scaled model without hole (Fig. 6). These three model types will share the same front design, as shown in Fig. 3.

In this study, since the size of the container model is fixed, and the material selectivity of 3D printing is also relatively small, we do not strictly require the weight of the model to meet a certain

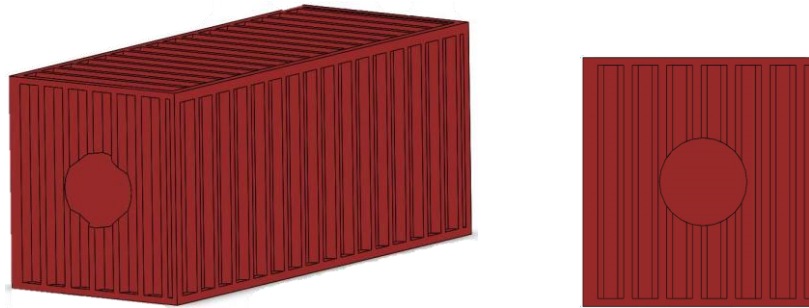


Fig. 4 Back view of Model Type I –with a centric hole



Fig. 5 Back view of Model Type II - with an eccentric hole

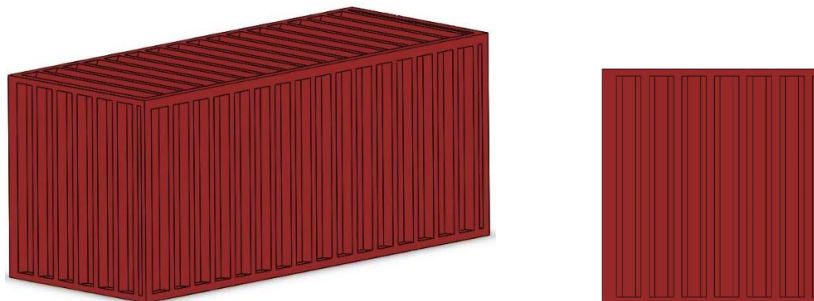


Fig. 6 Back view of Model Type III – with no hole

Table 1 Original container vs. Container model

	Length (mm)	Width (mm)	Height (mm)
Standard 20ft container	6058	2438	2591
Scaled container model	169	68	72

similarity with the actual loading situation. To simplify the problem, we only require that the average density is heavier than water to ensure that the model can sink. In this manner, the trajectories after sinking can be studied. Of course, we also considered different center of gravity positions. More detailed discussions can be found in section 2.4.

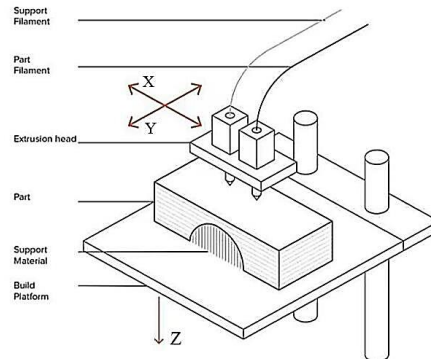


Fig. 7 Schematic diagram of FDM (Varotsis 2021)



Fig. 8 Raw surface of the container model printed by FDM printer

To import the SolidWorks model into the 3D printer, we only need to save the original file as an STL file. This ASCII or binary format file can describe the surface geometry of 3D objects as primitive, unstructured triangular surfaces.

### 2.2.3D Printing technology

The models were produced on a Stratasys F170 Fused Deposition Modeling (FDM) printer that uses a filament of plastic material to build 3D objects. The FDM process is the most common 3D printing method to produce parts and models comprised of ABS, PLA and other common thermoplastics. Before the FDM printing process begins, the 3D model is sliced into multiple layers based on a layered construction process to produce physical models. Then, the extrusion head—which can move in X and Y directions—locally heats the input material in the form of a plastic filament, causing local melting (Kozior and Kundera 2017). After depositing a layer of material, the build platform is lowered in the Z direction according to the specified layer thickness and the whole process is repeated until the entire model is completed. The finished products printed by FDM printer are both functional and durable, which makes it a popular process widely used in various industries, including mechanical engineering and parts manufacturers. Fig. 7 gives a schematic diagram of the FDM printer.

With the help of support filament and build material, FDM systems are capable of printing models with significant geometrical complexity. The support materials will support overhanging structures during printing and help maintain the structural integrity of parts until they are removed by dissolving with an appropriate solvent (Chennakesava and Narayan 2014).

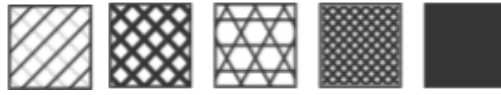


Fig. 9 Schematic diagram of infill style (Stratasys F170 Protocol 2020)

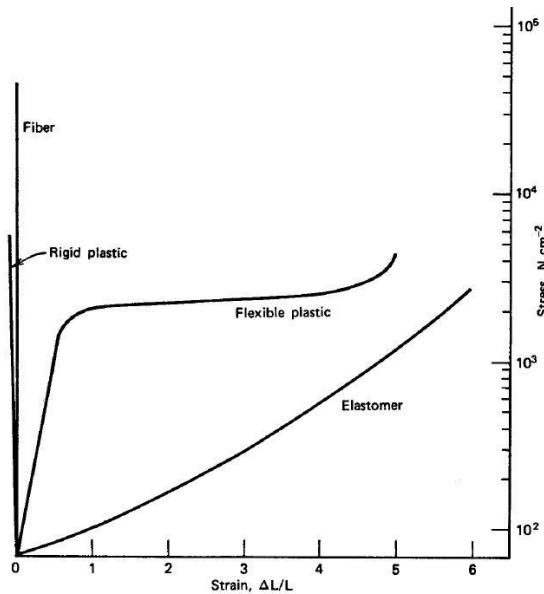


Fig. 10 Stress-Strain plots (O dian 2004)

Like many other 3D technologies, raw FDM parts can display quite visible layer lines on certain objects (3D INSIDER, 2021). Fig. 8 is the raw surface of our printed container models. The layer lines are noticeable but not rough to the touch. A common way to reduce the surface roughness of FDM parts is by sanding and polishing the model by hand after printing.

The Stratasys F170 system provides 5 options to choose from when selecting an infill style, which are sparse, sparse with double dense, hexagram, sparse with high density and solid, as shown in Fig. 9 from left to right, respectively.

In our case, all models use the sparse infill setting with high density. This kind of infill style deposits filament material in a single direction per layer. Compared to fully dense infill settings, it is best to produce parts with high structural integrity with reduced build time and part cost.

### 2.3 Material

All models are made of acrylonitrile styrene acrylate (ASA) material, which is a thermoplastic elastomer. According to Odian (2004), elastomers are the group of polymers that are prone to very large reversible elongation under relatively low stress. This requires the polymer to be completely (or almost completely) amorphous with a low glass transition temperature and low secondary forces so as to obtain high polymer chain mobility. Meanwhile, thermoplastic is defined as a polymer that can be melted and recast almost indefinitely. These characteristics make ASA suitable to be melted and printed as a 3D printing material.

Table 2 Basic properties of ASA

Density	1.00 - 1.24 g/cm <sup>3</sup>
Hardness	75 - 119
Modulus of Elasticity	1.45 - 2.80 GPa
Strength at break	47 - 56 MPa
Melt Temperature	170 - 280°C
Drying Temperature	70 - 100°C

Table 3 Properties of fillers

Filler	Density (kg/m <sup>3</sup> )	Mass (kg)
Aluminum	2317.99	0.18
Steel	7756.83	0.59

Fig. 10 presents the Stress-Strain plots for a typical elastomer, a flexible plastic, a rigid plastic, and a fiber, where the modulus of a polymer is the initial slope of each curve; the tensile strength and ultimate elongation are the highest stress and elongation values, respectively (Odiان 2004). Elastomer has a smooth Stress-Strain curve, which almost obeys the general Hooke's law with no strain hardening region or necking region being observed. This can ensure that the model is not easily damaged during the drop test.

Also, ASA is amorphous and has mechanical properties similar to ABS plastics. However, its characteristics are much less affected by outdoor weathering. ASA parts have good chemical and heat resistance and high impact strength and color fade/aging/yellowing resistance, even at low temperatures. Table 2 gives some basic properties of ASA.

#### 2.4 Model filling

Two materials, e.g., aluminum and steel, are used to fill the model. After calculations, it was found that when aluminum is filled into the model, the density of the whole model is slightly larger than that of water. This is very helpful for observing the trajectory of the container model in the hydrostatic test. As a result, aluminum is selected. Meanwhile, to highlight the comparison between experimental models, steel is chosen as another filling material because of its high availability and larger density. Table 3 gives the basic properties of these two fillers.

#### 2.5 Formula to estimate the probability per area

Now that we have the experimental data of where the object falls, we prepare to sort out the specific falling point and calculate the angular deviation,  $\alpha$ , as well as lateral deviation,  $\delta$ , to compare with the data given in the Det Norske Veritas (DNV) rule (2010).

According to Fig. 11, the deviation  $\delta$  can be expressed as

$$\delta = h \cdot \tan \alpha \quad (1)$$

The angular deviation is

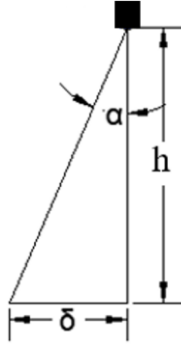


Fig. 11 Schematic diagram of angular deviation and lateral deviation

$$\alpha = \arctan\left(\frac{\delta}{h}\right) \quad (2)$$

With the experimental data, we could also obtain the distribution of falling container models in a different area, from which we could calculate the hit probability. Assuming landing locations on the horizontal position of the bottom to be normally distributed, we could have

$$p(x) = \frac{1}{\sqrt{2\pi}\delta} e^{-\frac{1}{2}\left(\frac{x}{\delta}\right)^2} \quad (3)$$

Similar to DNV rule (2010), the probability  $P_r$  within a ring area with an inner radius  $r_i$  and an outer radius  $r_o$  can be found by

$$P_r = P(r_i < r \leq r_o) = P(r \leq r_o) - P(r \leq r_i) \quad (4)$$

The ring area  $A_r$  can be easily calculated as

$$A_r = \pi(r_o^2 - r_i^2) \quad (5)$$

The probability per area,  $P_{A_r}$ , is defined by dividing the hit probability  $P_r$  by the area of a circle with radius  $r$

$$P_{A_r} = \frac{P_r}{A_r} \quad (6)$$

## 2.6 Experimental setup for drop tests

A series of drop tests were performed in the towing tank at the University of New Orleans (UNO). Fig. 12(a) is an overview of the horizontal grid mat laid on the bottom of towing tank to measure the final landing locations of container models. Fig. 12(b) shows a vertically installed grid, which can be used to roughly track and record the position of the container model at each moment. In addition, Fig. 12(b) also shows a small white device used to adjust the drop angle to implement the three drop angles in this study easily.

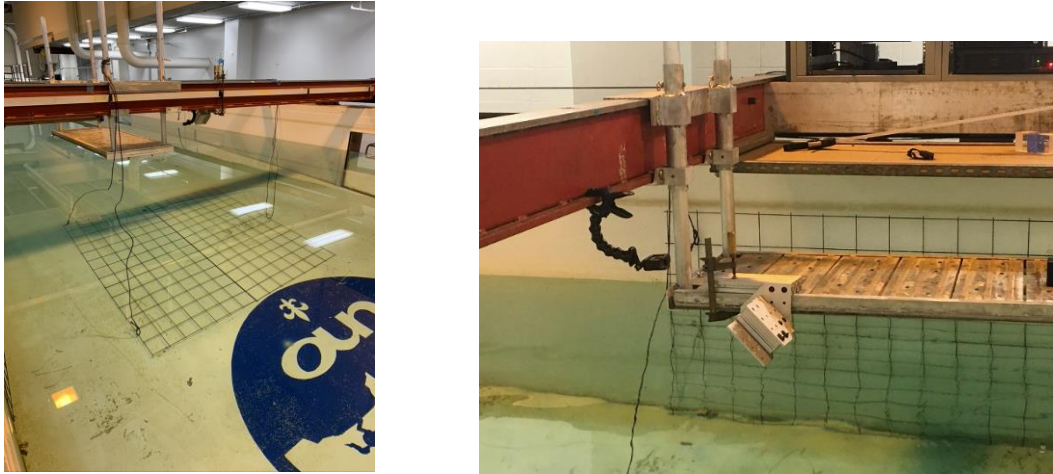


Fig. 12 (a) Overview of grid mat laid on the bottom of towing tank (left) and (b) The observing system (right)



Fig. 13 Six 3D-printed models

### 3. Results and discussions: Properties of 3D-printed container models

A total of 6 models are printed, 4 with holes and 2 solid models, as shown in Fig. 13.

We use a Vernier caliper to measure the basic dimensions of the 3D printed container models multiple times. The averaged measured value will be compared with the targeted dimensions defined in SolidWorks.

In addition, the drainage method is used to measure the displaced volume of the model to estimate the density. Fig. 14 shows how to find the COG of these container models, and each model is measured multiple times to reduce the measurement error.

#### 3.1 Dimensions and difference percentage of 3D-printed container models

Table 4 shows the data obtained via the Vernier caliper. The relevant definitions of dimensions are illustrated in Fig. 15. The difference between each model is quite small.

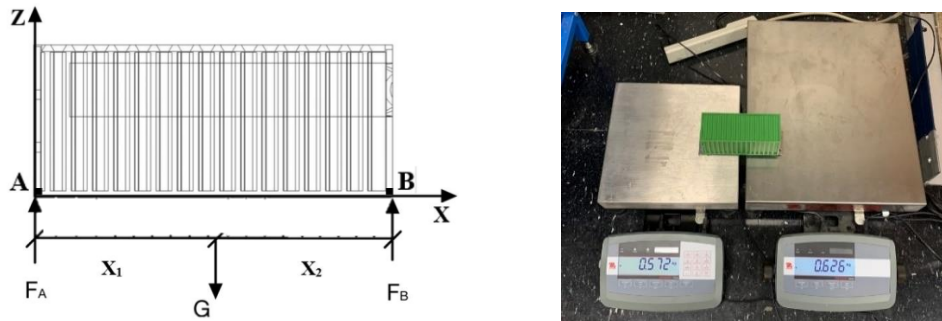


Fig. 14 (a) Schematic diagram of balance (left) and (b) Equipment used for actual measurement (right)

Table 4 Dimensions of container models

Model No.	Position of the hole	Filler	a (mm)	b (mm)	c (mm)	d (mm)	e (mm)	f (mm)	g (mm)	h (mm)
1	Centric	Aluminum	68.30	72.20	169.50	22.80	26.40	20.90	24.10	23.10
2		Steel	68.00	72.10	169.50	22.10	26.10	19.80	23.50	23.40
3	Eccentric	Aluminum	68.00	72.10	169.60	23.00	25.00	20.00	38.30	8.90
4		Steel	68.00	72.10	169.70	22.70	25.40	19.90	38.10	8.80
5	No Hole	/	68.20	72.20	169.30	/	/	/	/	/
6		/	67.90	72.00	170.90	/	/	/	/	/

Table 5 Difference percentage of the model size

Model No.	Position of the hole	Filler	Difference percentage							
			da (%)	db (%)	dc (%)	dd (%)	de (%)	df (%)	dg (%)	dh (%)
1	Centric	Aluminum	0.44	0.28	0.30	2.47	3.94	2.70	3.17	0.60
2		Steel	0.00	0.14	0.30	0.67	2.76	2.70	0.60	0.69
3	Eccentric	Aluminum	0.00	0.14	0.36	3.37	1.57	1.72	0.52	4.71
4		Steel	0.00	0.14	0.41	2.02	0.00	2.21	0.00	3.53
5	No Hole	/	0.29	0.28	0.18	/	/	/	/	/
6		/	0.15	0.00	1.12	/	/	/	/	/

Since the size of the original model is  $a \times b \times c = 68 \times 72 \times 169$  mm, it is important to confirm that the 3D printed model has sufficient accuracy or that the deviation is small enough. The calculated deviation percentages of the model size are shown in Table 5. We use  $d_a$  to  $d_h$  to represent the deviation percentage of a to h, respectively. It can be said that considering manual errors and mechanical errors, the actual parameters of printed models are very close to the designed parameters and meet our requirements.

### 3.2 COG of 3D printed container models

Based on geometry and mass density information, we can calculate the COG after container models are filled, as shown in Table 6. In this table,  $X_g, Y_g$  and  $Z_g$  are the coordinate values of the center of gravity in the coordinate system defined in Fig. 15. Here, we only measure Model No. 1 to Model No. 4, filled with aluminum and steel. Model No. 5 and Model No. 6 are so light that they can float on the water, so they are not used in the drop test.

Table 6 Estimated COG after filling

Model No.	Position of the hole	Filler	Measured center of gravity (mm)		
			$X_g$	$Y_g$	$Z_g$
1	Centric	Aluminum	85.32	34.09	35.69
2		Steel	88.53	33.50	35.80
3	Eccentric	Aluminum	85.97	34.49	37.84
4		Steel	88.53	33.68	42.53

Table 7 Eccentricity after filling

Model No.	Position of the hole	Filler	Eccentricity from measured geometric centroid (mm)		
			$X_e$	$Y_e$	$Z_e$
1	Centric	Aluminum	0.57	0.06	0.40
2		Steel	3.78	0.50	0.25
3	Eccentric	Aluminum	1.04	0.34	1.74
4		Steel	3.68	0.32	6.48

Table 8 Total mass/density before and after filling

Model No.	Position of the hole	Filler	Total mass before fill (kg)	Total mass after fill (kg)	Density before fill ( $\text{kg}/\text{m}^3$ )	Density after fill ( $\text{kg}/\text{m}^3$ )	Increased ratio
1	Centric	Aluminum	0.65	0.83	826.14	1053.30	27.50%
2		Steel	0.60	1.20	758.88	1519.04	100.17%
3	Eccentric	Aluminum	0.65	0.83	826.14	1053.30	27.50%
4		Steel	0.59	1.19	752.54	1506.35	100.17%

Also, we have calculated the eccentricity of these container models after filling and organized the data in Table 7. In this table,  $X_e$ ,  $Y_e$  and  $Z_e$  are the offsets of the center of gravity from the center position shown in Fig.15, respectively.

Table 8 shows the densities and mass of Models No. 1 - No. 4 before and after filling. It shows that the density is increased by 27% if the filling material is aluminum and 100% for steel. Thus, the four models can be used to represent four significantly different loading conditions.

In this study, it is assumed that different COG positions shown in Table 5 correspond to six different loading conditions. In the future experimental tests, we will try to investigate the influence of different factors on the falling trajectory pattern of container models. Since these are all small-scale models, we do not try to quantitatively estimate the falling trajectories of actual containers based on the Froude law or Reynolds law in this paper. This will be carried out in future work.

#### 4. Results and discussions: Analysis of experimental data from drop tests

Fig. 16 - 19 show the top views of landing locations of Model No. 1 to Model No. 4, respectively. In these figures,  $x$  represents the distance along the length of towing tank, and  $y$  represents the lateral displacement. The drop angle  $45^\circ$  is in the positive  $x$ -direction.

The four models were dropped at UNO's towing tank at three different drop angles -  $0^\circ$ ,  $45^\circ$  and  $90^\circ$ , 20 times for each angle, so the total number of drops is 240. It should be

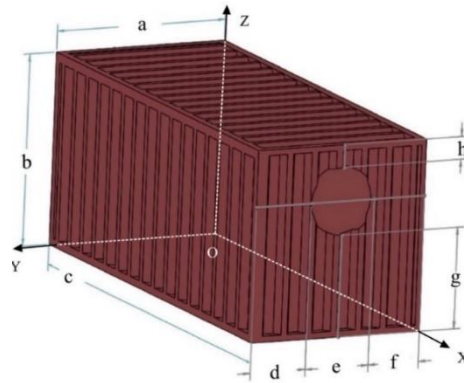
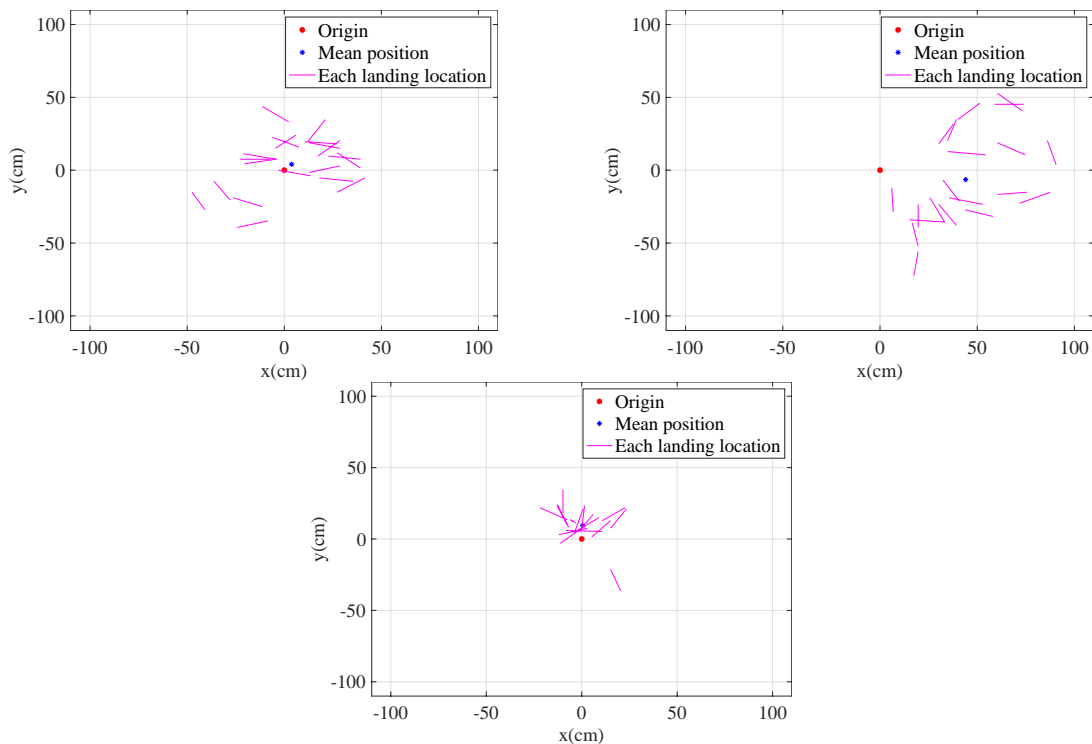


Fig. 15 Dimension definition of the container model

Fig. 16 Landing location distribution of Model No. 1 at  $0^\circ$  (top left – ‘a’),  $45^\circ$  (top right – ‘b’) and  $90^\circ$  (bottom – ‘c’)

addressed that the time interval between each test usually depends on whether the waves originated from the initial sinking of previous tests have decayed or not. In other words, we try to ensure that we perform the drop tests in calm water. However, due to many tests, it is difficult to remove various types of external noise, including very small waves from previous tests, and the waves reflected by the tank’s wall, etc, though the time interval between each drop test is long enough. Therefore, considering that these random noises are inevitable, we repeat 20 times for each model at each drop angle.

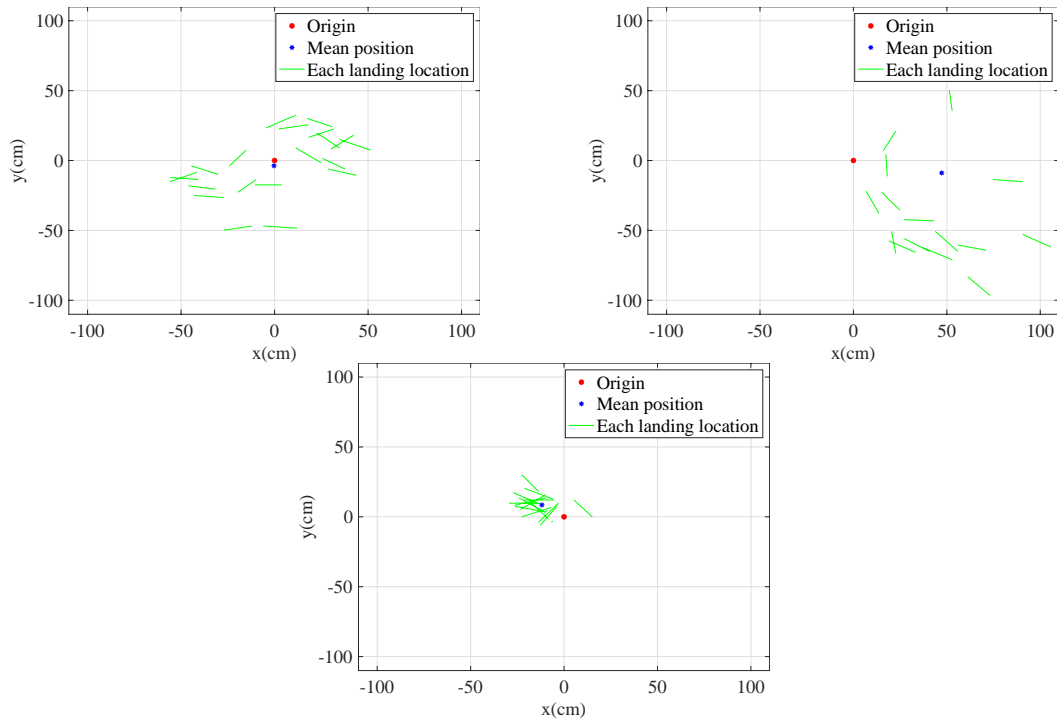


Fig. 17 Landing location distribution of Model No. 2 at 0° (top left – ‘a’), 45° (top right – ‘b’) and 90°(bottom – ‘c’)

Table 9 Statistical results of landing locations for each model

Model No.	Drop angle	Mean(cm)		STD(cm)		Mean(cm)		STD(cm)	
		x	y	x	y	r	r	r	r
1	0°	3.8	4.1	22.8	18.4	27.3	10.4		
	45°	44.0	-6.5	22.6	31.9	55.8	18.4		
	90°	0.5	9.5	9.9	10.9	15.3	8.0		
2	0°	-0.3	-3.8	30.6	22.3	35.5	10.9		
	45°	47.2	-8.9	25.0	36.9	74.5	30.1		
	90°	-11.8	8.5	7.4	6.2	16.2	6.5		
3	0°	-0.7	6.0	4.4	19.3	19.2	6.5		
	45°	43.7	3.6	9.4	24.4	50.0	8.8		
	90°	-38.6	4.5	4.9	11.1	40.3	4.9		
4	0°	-0.1	-1.0	10.1	23.9	25.0	4.3		
	45°	40.8	5.1	7.3	25.6	47.3	11.5		
	90°	-46.5	4.3	8.2	6.9	47.1	8.4		

Note:  $r = \sqrt{x^2 + y^2}$ , and it represents the radius of landing location

The drop angle is a very important factor since it affects the degree of dispersion of those landing locations. A 90-degree drop angle usually corresponds to a more concentrated landing location distribution, as can be observed from Fig. 16(c), Fig. 17(c), Fig. 18(c), and Fig. 19(c). Accordingly,

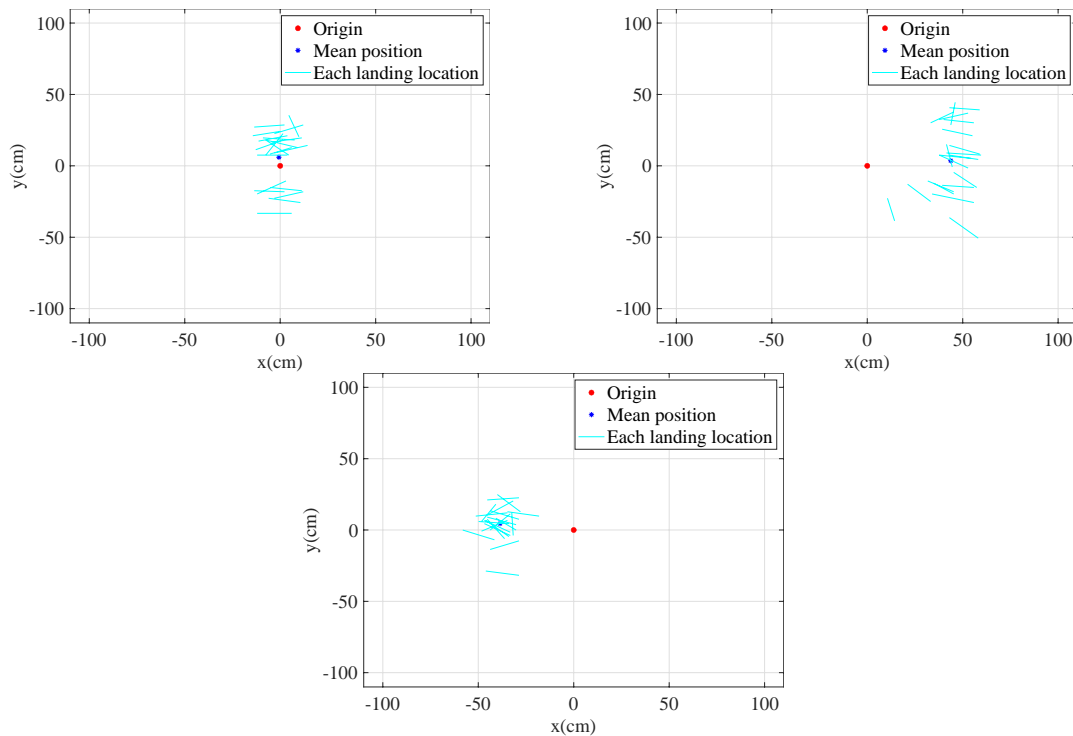


Fig. 18 Landing location distribution of Model No. 3 at 0° (top left – ‘a’), 45° (top right – ‘b’) and 90° (bottom – ‘c’)

the relatively smaller standard deviation (STD) of radius can also be found in Table 9; that is, 8.0 cm, 6.5 cm, 4.9 cm, and 8.4 cm, respectively. It may be because the 90-degree drop angle means the smallest touch area when compared with all the other drop angles. The larger the contact area between the model and the calm water surface, the greater is the interference caused by the entry of water, indicating that it is more likely to cause the surge velocity along the length direction and rolling rate in the water, thereby causing more significant drift.

In addition, Models No. 3 and No. 4 have an eccentric COG in Z direction, if compared with Models No. 1 and No. 2, which have a centric COG in Z direction. Such an eccentricity can cause a greater drift but more concentrated distribution, as shown in Figs. 18 and 19, if compared with Figs. 16 and 17, especially for 90-degree case. This could be further validated by a greater mean value of the radius, but smaller STD, as shown in the last two columns of Table 9.

It should be also addressed that the density of Model No. 2 is about 1519.04 kg/m<sup>3</sup>, about 44.22% greater than Model No. 1 with 1053.30 kg/m<sup>3</sup>, as shown in Table 8. Similarly, the density of Model 4 is about 1506.35 kg/m<sup>3</sup>, about 43.01% greater than Model No. 3 with 1053.30 kg/m<sup>3</sup>. The density does strongly affect the average time for landing, as clearly summarized in Table 10. Model No. 2 needs much less time to touch the tank bottom if compared with Model 1 for all the three drop angles, and similar findings can be also applied to Model No. 4 and Model No. 3.

Fig. 20(a) shows a sample scenario of landing location of four container models, and Fig. 20(b) is postprocessed in MATLAB by putting all the 240 landing locations in one figure.

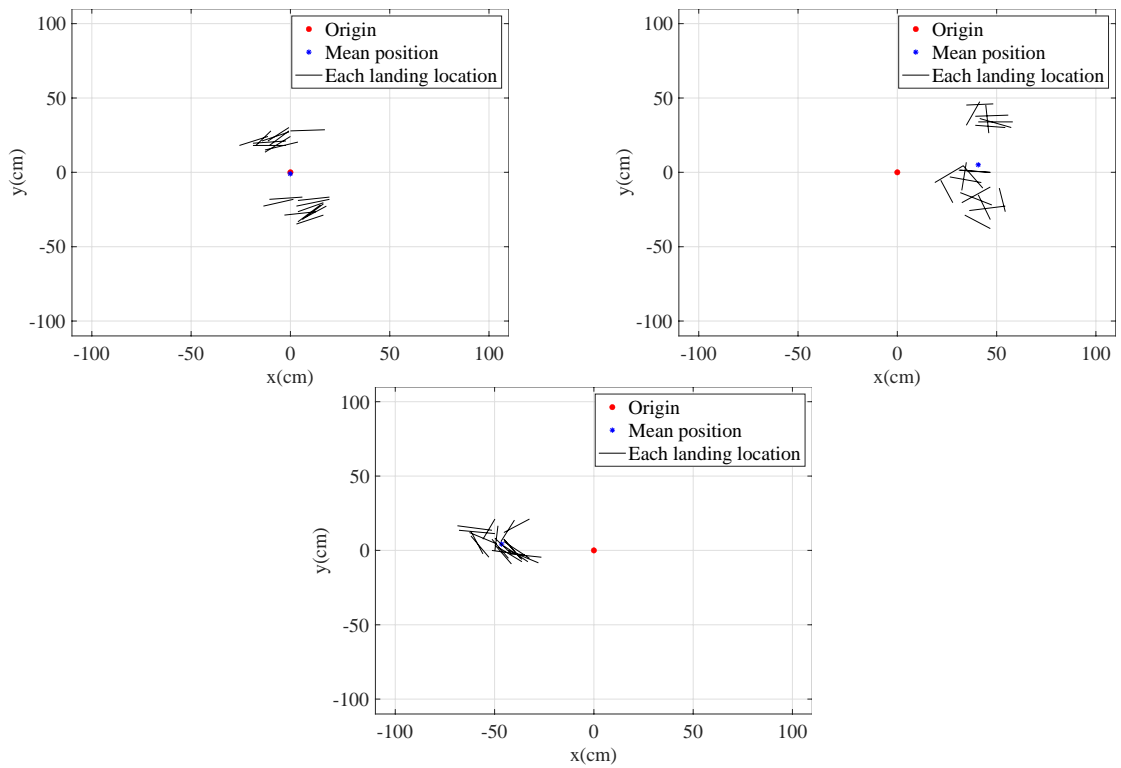


Fig. 19 Landing location distribution of Model No. 3 at 0° (top left – ‘a’), 45° (top right – ‘b’) and 90°(bottom – ‘c’)

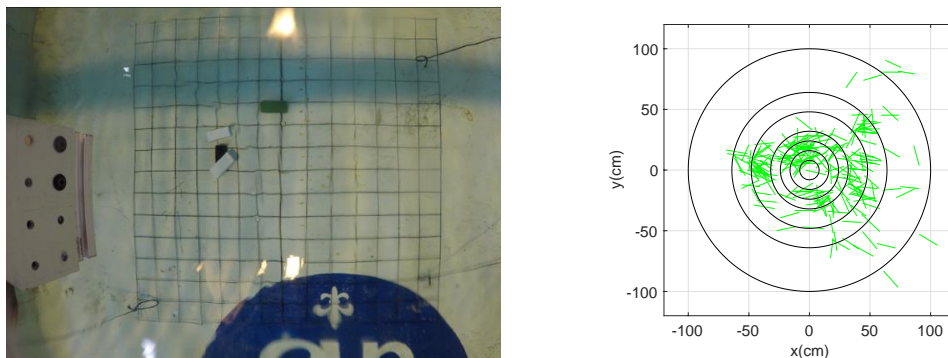


Fig. 20 (a) A scenario of landing location of four container models (left) and (b) Landing location distribution (right)

Table 10 Average time for landing

Model No.	Elapsed time (s)		
	0°	45°	90°
1	3.71	3.21	1.94
2	1.8	2.04	0.92
3	3.77	3.53	2.07
4	1.99	1.93	1.25

Table 11 Angular deviation and its corresponding lateral deviation

$\alpha$ (°)	0	2.54	5.08	7.59	10.08	14.93	19.57	29.05
$\delta$ (cm)	0	8	16	24	32	48	64	100

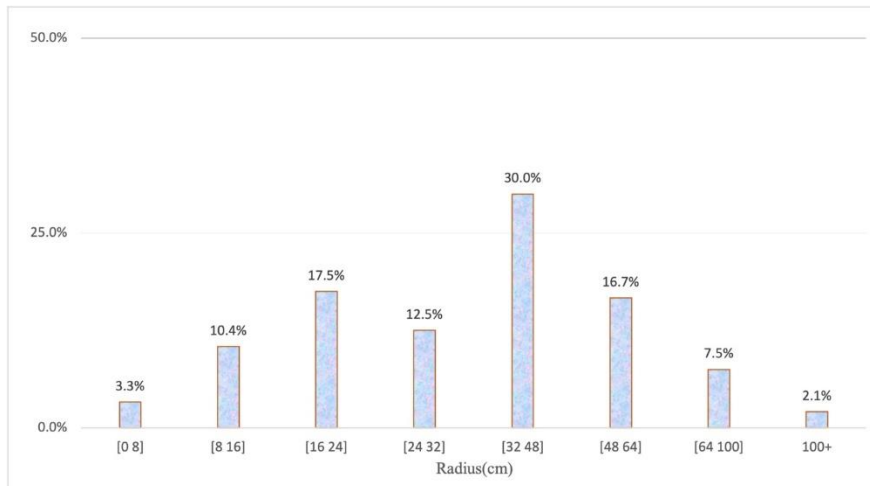


Fig. 21 Probability histogram of dropped container models

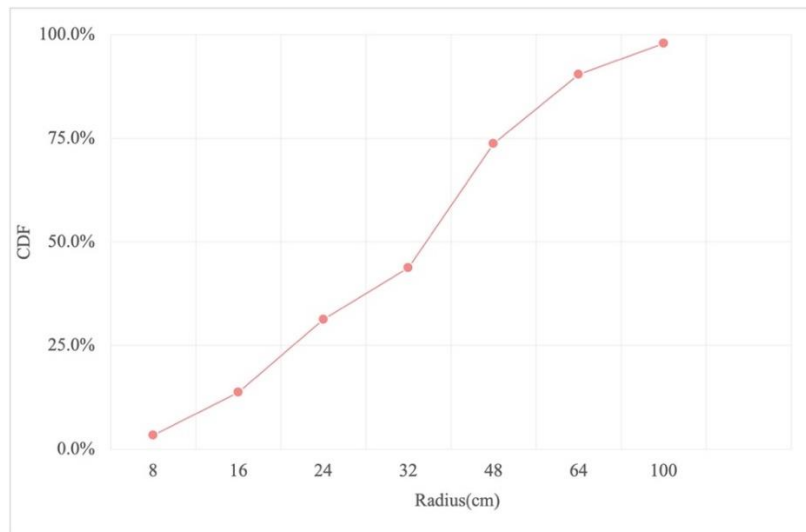


Fig. 22 Cumulative distribution function of dropped container models

Therefore, the probability of falling into a certain interval can be calculated by dividing the number of times falling in each interval by 240, as marked in Fig. 21. This is the so-called probability density function. From Fig. 21, it can be observed that the container models will drop into the interval [32 cm to 48 cm] most probably – about 30.0% chance, with the corresponding angle [10.08°, 14.93°]. This probability density function can be further integrated to get the cumulative distribution function (CDF), as shown in Fig. 22.

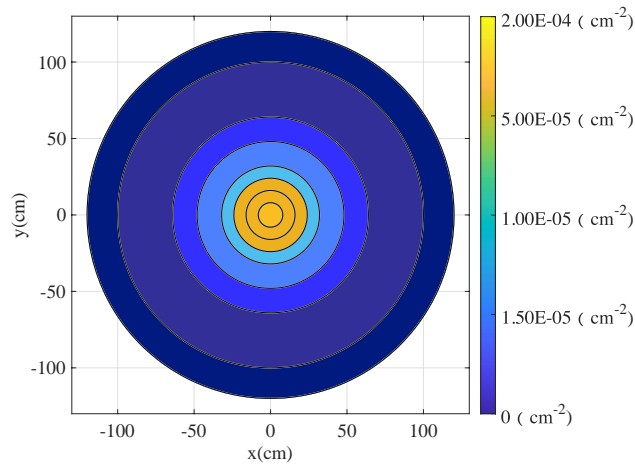


Fig. 23 Probability per area,  $P_{A_r}$ , based on the experimental data

From Fig. 22, it can be found that the probability of more than 50%, the container model will fall within a radius of 36 cm; the probability of more than 80%, the container model will fall within a radius of 53 cm; the probability of more than 90%, the container model will fall within the radius of 62 cm; in addition, the probability of the container model falling outside the radius of 100 cm is almost zero.

Referring to the definition of these two parameters—the angular deviation and lateral deviation in the DNV rule (2010) specifications and the calculated results listed in Table 11—these experimental data indicate that for relatively light square objects, there is a high probability that these objects will enter the water surface with a drop angle of  $15^\circ$  even  $30^\circ$ . It should be noted that all the small-scaled models are less than 2 kg, much lighter than the actual full-scale offshore structures categorized in DNV rule (2010). In the guidance (DNV 2010), the angular deviation is  $2^\circ$  for weight much greater than 8 tonnes,  $3^\circ$  for weight about 8 tonnes and  $5^\circ$  for weight between 2 tonnes and 8 tonnes. All these indicate that the angular deviation of light objects is often smaller, and it could be larger for heavy objects. This is completely consistent with our intuition.

These experimental data have strong practical value. With reference to DNV rule (2010) and Yasserli (2014), we can obtain the plot of probability per area,  $P_{A_r}$ . The results are shown in Fig. 23. These results can be used in further risk analysis, including pipeline protection design and so on.

In the experimental tests, it is also found that rolling has an important influence on the lateral displacement  $y$ . The initial rolling rate depends on the multiple factors, including the container's vertical speed and angle of entry. This finding is consistent with those reported for cylindrical objects (Aanesland, 1987, Yu 2020b). Inspired by the work of cylindrical objects, the experimental test of this research aims to study the falling mechanism of box-shaped objects. This experiment may be the earliest experiment to test the trajectory of box-shape objects. Considering that the 3D-printed container models are similar to the real container, the experimental data from these tests can be applied to real maritime salvage operations.

Finally, the falling pattern of container models can be vividly displayed in Fig. 24. This experiment shows that the sunken container model will fall along a curve, like an inverted quadratic or even higher-order parabola. Meanwhile, the lateral displacement of those models is also observed.

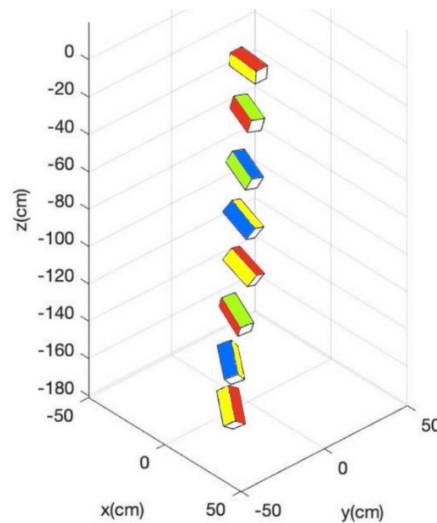


Fig. 24 Schematic diagram of the falling pattern of dropped container model

This value mainly depends on the rolling rate, which largely depends on the interaction when entering the water. It can be further observed that these models usually should flip 0-5 cycles, with a water depth 1.8 meters.

In addition, the aspect ratio is about 2.48 ( $= 6058 / 2438$ ), much smaller than 5.0, which is the minimum ratio for the slender-body cylindrical objects in offshore engineering. Obviously, this falling pattern of container models is much simpler than the proposed six patterns for cylindrical objects in Aanesland (1987).

This plot in Fig. 24 are combined with the falling time and summarized in Table 10 to understand the fundamental falling pattern of box-shape objects at different drop angles.

## 5. Conclusions

In this study, six container models made of acrylonitrile styrene acrylate (ASA) are successfully manufactured by a Stratasys F170 FDM printer. They represent three different loading conditions with different densities and COG, and there are two samples for each condition. After measurement, the relative error between the actual geometric dimensions and the pre-designed dimensions is very small, which fully meets the requirements of experimental tests in the field of naval architecture and offshore engineering. In addition, four of the models with a hole are filled with heavier materials, such as steel or aluminum, to make their average density greater than water. The measured results of COG and the density agree with the theoretical design values, which also fully meet the accuracy requirements of the test. Overall, additive manufacturing (also called “3D printing”) provides a fast, efficient, and more economical way to make small-scaled maritime structural models.

Furthermore, four container models have been dropped into the calm water in UNO’s towing tank. The effects of various factors, such as drop angle, center of gravity and mass density, etc. on the trajectories of the dropped container models have been comprehensively investigated in an experimental way. In addition, the falling pattern of container models has been tentatively proposed

and summarized. The drop test results also reveal that the impact of the water entry can cause a certain initial rolling velocity, which may significantly impact the lateral displacement and then affect the final landing position. More detailed research work about water entry of dropped containers should be part of future work but not the focus of this article.

The probability histogram from the experimental data provides an intuitive and direct distribution map in accordance with the existing specification (DNV, 2010), and this has certain significance for discovering and salvaging containers. Finally, the results about probability per area will be helpful for risk management and risk area division during container loading and unloading.

Except for the drop tests in calm water, we have also performed the drop tests in regular waves, and we are still postprocessing the results. The effects of current and internal contents inside container models are also worth discussing in the future.

## Acknowledgments

This work is currently supported in part by the US National Science Foundation under grant number OIA-1946231, the Louisiana Board of Regents for the Louisiana Materials Design Alliance (LAMDA) through a preparatory seed grant, and UNO ORSP office. It was also supported by NSF EPSCoR RII Track-1 Co-operative Agreement OIA-1541079, Louisiana Board of Regents for Consortium for Innovation in Manufacturing and Materials (CIMM).

## References

- 3D INSIDER (2021), The 9 Different Types of 3D Printers. <https://3dinsider.com/3d-printer-types/#sla> (accessed July, 2021).
- Aanesland, V. (1987), Numerical and experimental investigation of accidentally falling drilling pipes. 19th Annual OTC in Houston, Texas.
- American Bureau of Shipping (ABS) (2017), ABS Advisory on Additive Manufacturing. USA.
- American Bureau of Shipping (ABS) (2018), Guidance Notes on Additive Manufacturing. USA.
- Arnold, J., Do, J.Y.N., Smith, L.C., Poltavets, V. and Smith D.A. (2021), “Extrusion of shrimp shell-polylactic acid composites: Dataset for the impact of surfactants on their morphology and thermal properties”, *Data in Brief*, **36**, 107059. <https://doi.org/10.1016/j.dib.2021.107059>.
- Arnold, J., Sarkar, K. and Smith, D. (2020), “3D printed bismuth oxide-polylactic acid composites for radio-mimetic computed tomography spine phantoms”, *J. Biomedical Mater. Res. Part B Appl. Biomater.*, <https://doi.org/10.1002/jbm.b.34744>.
- Baumers, M., Dickens, P., Tuck, C. and Hague, R. (2016), “The cost of additive manufacturing: machine productivity, economies of scale and technology-push”, *Technol. Forecast. Social Change*, **102**, 193-201. <https://doi.org/10.1016/j.techfore.2015.02.015>.
- Bernhofen, D.M., El-Sahli, Z. and Kneller, R. (2015), “Estimating the effects of the container revolution on world trade”, *J. Int. Economics*, **98**, 36-50. <https://doi.org/10.1016/j.jinteco.2015.09.001>.
- Chawa, P.K. and Mukkamala, S.K. (2018), “Design and analysis of shipping container made of honeycomb sandwich panels (Master thesis), Department of Mechanical Engineering, Blekinge Institute of Technology, Karlskrona, Sweden.
- Chennakesava, P. and Narayan, Y.S. (2014), “Fused deposition modeling – Insights”, *Proceedings of the International Conference on Advances in Design and Manufacturing (ICAD&M'14)*.
- Det Norske Veritas (DNV) (2010), DNV Recommended Practice: Risk Assessment of Pipeline Protection, DNV- RP- F107.

- Ford, S. and Despeisse, M. (2016), "Additive manufacturing and sustainability: an exploratory study of the advantages and challenges", *J. Cleaner Production*, **137**, 1573-1587. <https://doi.org/10.1016/j.jclepro.2016.04.150>.
- Franchetti, M. and Kress, C. (2016), "An economic analysis comparing the cost feasibility of replacing injection molding processes with emerging additive manufacturing techniques", *Int. J. Adv. Manuf. Technol.*, **88**, 2573-2579. <https://doi.org/10.1007/s00170-016-8968-7>.
- Frey, O.T. and DeVogelaere, A.P. (2014), *The Containerized Shipping Industry and the Phenomenon of Containers Lost at Sea. Marine Sanctuaries Conservation Series ONMS14-07*. U.S. Department of Commerce, National Oceanic and Atmospheric Administration, Office of National Marine Sanctuaries, Silver Spring, MD. 51 pp.
- Koh, A. (2021), *Shipping Containers Fall Overboard at Fastest Rate in Seven Years* [WWW Document]. URL: <https://www.bloomberg.com/news/articles/2021-04-26/shipping-containers-plunge-overboard-as-supply-race-raises-risks> (accessed August, 2021).
- Kozior, T. and Kundera, C. (2017), "Evaluation of the influence of parameters of FDM technology on the selected mechanical properties of models", *Procedia Eng.*, **192**, 463-468. <https://doi.org/10.1016/j.proeng.2017.06.080>.
- Milewski, J.O. (2017), *Additive Manufacturing of Metals from Fundamental Technology to Rocket Nozzles, Medical Implants, and Custom Jewelry*. Volume 258.
- Ngo, T.D., Kashani A., Imbalzano G., Nguyen K.T.Q. and Hui, D. (2018), "Additive manufacturing (3D printing): A review of materials, methods, applications and challenges", *Compos. Part B: Eng.*, **143**, 172-196. <https://doi.org/10.1016/j.compositesb.2018.02.012>.
- Odian, G. (2004), *Principles of Polymerization*, Fourth Edition. College of Staten Island, City University of New York, Staten Island, New York. <https://doi.org/10.1002/047147875X>.
- Stratasys F170 Protocol (2020), UC Berkeley Mechanical Engineering, <https://me.berkeley.edu/wp-content/uploads/2020/07/Stratasys-f170-Protocol.pdf> (accessed August, 2021)
- Varotsis, A.B. (2021), *Introduction to FDM 3D printing* [WWW Document], <https://www.hubs.com/knowledge-base/introduction-fdm-3d-printing/#characteristics> (accessed August, 2021).
- Xiang, G., Birk, L., Yu, X. and Lu, H. (2016), "Numerical study on the trajectory of dropped cylindrical objects", *Ocean Eng.*, **130**, 1-9. <https://doi.org/10.1016/j.oceaneng.2016.11.060>.
- Xiang, G. and Xiang, X.B. (2021), "3D trajectory optimization of the slender body freely falling through water using cuckoo search algorithm", *Ocean Eng.*, **235**, 109354. <https://doi.org/10.1016/j.oceaneng.2021.109354>.
- Yasseri, S. (2014), "Experiment of free-falling cylinders in water", *Underw. Technol.*, **32**(2), 177-191.
- Yu, X., Li, L., Xiong, Z. and Kang, S. (2020a), "Hit probability of cylindrical objects dropped on pipelines in offshore operations", *J. Pipeline Syst. – Eng. Practice*, **11**(4), 04020048.
- Yu, X., Meng, H., Zhen, Y. and Li, L. (2019), "Trajectory prediction of cylinders freely dropped into water in two dimensions based on state space model", *Ocean Eng.*, **187**, 106154.
- Yu, X., Xiang, G., Collopy, H. and Kong, X. (2020b), "Trajectory tracking of a model rocket falling into the towing tank: experimental tests versus numerical simulations", *J. Aerosp. Eng.*, **33**(5), 04020056. [https://doi.org/10.1061/\(ASCE\)AS.1943-5525.0001172](https://doi.org/10.1061/(ASCE)AS.1943-5525.0001172).